

# A NOVEL HYBRID MODEL OF REINFORCED CONCRETE DEEP BEAMS WITH CURVED HYBRIDIZATION

Qasim Mohammed Shakir\*, Hawraa Khalid Hannon

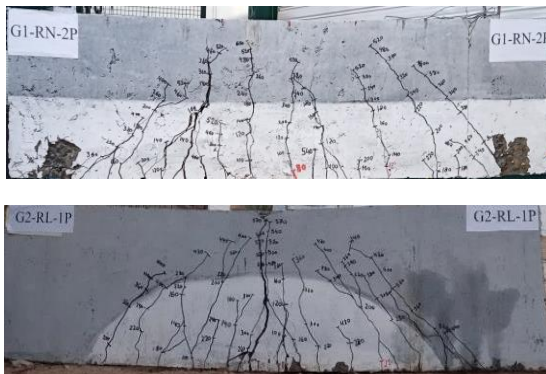
Civil Engineering Department, University of Kufa, Najaf, Iraq

## Article history

Received  
16 September 2021  
Received in revised form  
15 February 2022  
Accepted  
15 November 2022  
Published Online  
23 February 2023

\*Corresponding author  
qasimm.alabbasi@uokufa.edu.iq

## Graphical abstract



## Abstract

In the present study, a new model of hybrid deep beams has been proposed and discussed. Six specimens are tested experimentally with two types of loading which are one-point and two-point loading and two hybridization models for concrete section. It is aimed from this study to search for the optimum distribution of the concrete types of the hybrid deep beams such that the lowest cost and weight to be reached with keeping the capacity without significant reduction. All specimens had the same dimensions, overall span of 1700 mm, 180 mm wide and 450 mm overall depth and the same steel reinforcement details. Results showed an increase in the capacity in the horizontal and the arched hybrid model by 27.6% and 39%, respectively, with one-point system. Moreover, toughness, enhanced by 44% and 131% for the two models respectively whereas, stiffness enhanced by 6.5% and 34.2% respectively and ductility enhanced by 0% and 31.2% respectively. For tests under two point loads, capacity enhanced by 34% and 36.9%, respectively, Toughness increased by 188% and 301% respectively. Stiffness enhanced by 7.5% and 29.4% respectively. Ductility enhanced by 40.3% and 95.1% respectively.

**Keywords:** Deep beams, hybrid deep beams, reactive powder reinforced concrete, lightweight concrete, flexural and diagonal cracks, stiffness

© 2023 Penerbit UTM Press. All rights reserved

## 1.0 INTRODUCTION

In some applications, beams are subjected to concentrated or distributed loads in a manner that may result in severe concentration of stresses within all the beam. Such beam are called by ACI318-19 code [1] as deep beam and are characterized by a limited value of shear span to overall depth ratio not more than (2.0), then to be considered as D-region as in corbel, dapped end, etc. [2-6]. Deep beam are used as transfer beams in high-rise building, column-bearing beams, bridges, tank walls and foundations

wall [7]. Many studies proved that the incorporation of steel fibers in concrete resulted in significant improvement in the general performance of the structural members in terms of reducing rate of cracking and deformation [8]. Consequently, steel fibers have been included in beams, slab, corbel, around web openings, dapped end [9-12]. In deep beam, steel fiber have been used to improve the shear strength [13-14]. The hybrid deep beam with several models of hybridization have been proposed to control the cost with keeping the acceptable performance for the deep beams. Several proposals

has been suggested including the horizontal hybridization. In 2014, Hassan [15] testing hybrid deep beams of the two layers of concrete (ultra-high performance concrete UHPC and normal concrete, UHPC used in compression of beams, show that the increase in the capacity of beam by increasing the thickness of the UHPC layer and the proportion of steel fibers used in concrete. Sada and Resan 2021 [16] used the trapezoidal section instead of the rectangular one. RPC (reactive powder concrete) has been used in various types of structural members [17-18].

Recently, RPC has been used in deep beams to improve the general performance. Amongst studies of RPC deep beam was the study of Muhaison, *et al.* 2018 [19] discussed the behavior of RPC deep beams with openings. Results proved that the ultimate strength and cracking load was enhanced by, and that inclusion opening reduced the ultimate load by (22-23)%. However, the high cost of the RPC constituent restricted the wide use in deep beam with RPC and to be in practical. Qasim and Hawraa [20] developed a novel model of hybrid deep beam that incorporated the merits of weight reduction, performance, and cost. Steel fiber concrete was used at the top layer, curved distribution of the concrete types has been adopted.

The present work represents a more improved version of the novel hybrid model presented in [20]. In this model, the reactive powder concrete has been used at the top layer which varied gradually along the beam to comply the requirements of flexural capacity at supports (D-region). Full section is made of RPC to accumulate the high concentration of stress and to control crushing due to the concentrated reaction and supports. This model may result in developing higher moment and shear capacities. Then, the need to NSC may be eliminated and replaced by LWC, concrete with recycled aggregate or low strength concrete without severe reduction in capacity, then, resulting in reduction in weight and cost of the produced deep beams and production of more sustainable members. Thus, The significance of the present work can be summarized as follows:

- 1) The curved RPC hybrid model may result improving the performance and increasing the capacity of the deep beams.
- 2) The proposed model may result in more economical sections by using the low strength concrete or smaller weight by using the light weight concrete within the lower part of the beam.
- 3) The proposed model may be extended to produce more sustainable model by using concrete with recycled aggregate.
- 4) More improved hybrid curved models may be proposed based on the concepts of tied arch, arching action and strut-and tie (STM) models.

## 2.0 METHODOLOGY

### 2.1 Specimens Description

The experimental program included testing six specimens, each two are identical in the internal detailing. Two systems of loading are adopted which are: One mid-span point load system and, two-points load system, applied at 210 mm on both side of center line of beam. The tested specimens are grouped into three sets: The first one represented the control specimens, which include beams made of NSC ( $f_{cu}=46\text{MPa}$ ). Such beam have been designed based on the STM model adopted by ACI318M-19 building code [1]. The second set was made of hybrid configuration of (RPC) at the top half layer and (NSC) at the bottom half layer. RPC had  $f_{cu}=93\text{MPa}$ , as shown in Figure 1(a).

The bases of the proposal is to improve the compression capacity such that more tensile strength may be equilibrated. The third set was made from reactive powder concrete and lightweight concrete (not NSC) with exception that the concrete have been distributed as in Figure 1(b) in a pattern that concrete of high strength RPC was used at the compression layer at which the B.M is dominant. Then, a higher tensile force is to be induced. Moreover, the concrete used at support region (D-region) was of the high strength RPC also, to avoid the failure at supports by local crushing that may occur within high level of loading if LWC is used. In the bottom layer of the mid span region, LWC has been used because this region is controlled by flexural stresses and that the location of N.A lies at less than ( $h/2$ ) from the top of the beam. It is to be mentioned that in the second set, the LWC was not used because of the expectation that the beams may fail in early stages of loading.

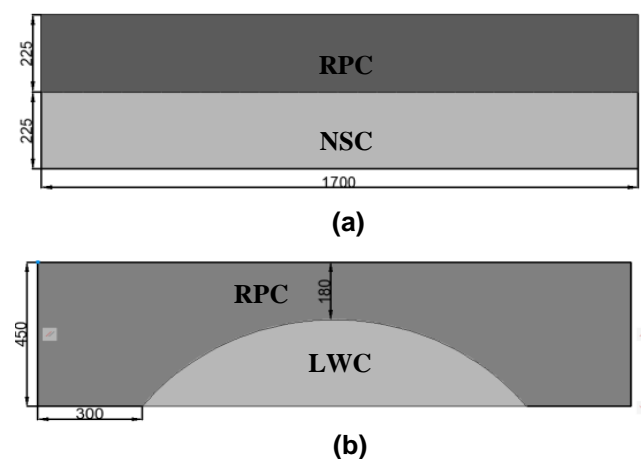


**Figure 1** a) horizontal hybrid deep beam, b) arched hybrid deep beam

A typical specimens has dimension 450 mm overall depth, 180 mm width and 1700 mm total length (with clear span of 1500 mm). The mid -point load system produce a value of ( $a/d$ ) of 1.67 while

that of two- points loading produce ( $a/d$ ) of 1.2. Table 1 shows the coding adopted for the tested specimens. Steel reinforcement consisted of three sizes,  $\varnothing 8 @ 130$  mm C/C for shear reinforcement,  $2\varnothing 10$  mm at top of the beam and  $3\varnothing 16$  mm at main tension steel reinforcement.

**Table 1** Coding of specimens

Coding	Definition of beam
CTRL-1P	Control under one point load
G1-RN-1P	Horizontal hybrid under one point load
G2-RL-1P	Arched hybrid under one point load
CTRL-2P	control under two point loads
G1-RN-2P	Horizontal hybrid under two point loads
G2-RL-2P	Arched hybrid under two point loads

## 2.2 Materials Used in Experimental Work

Ordinary Portland cement (CAR) was tested and conformed to the Iraqi Specification No. 5, 1984 [21]. washed natural sand was used as fine aggregate, natural Crushed gravel has been used in the normal concrete mix. The gravel was clean and saturated dry surface. The results of physical and chemical properties compliant with Iraqi specification No. 45/1984. [22], Table 2 and 3 shows physical and chemical properties of the sand and gravel respectively. Silica sand with a maximum particle size of 0.6 mm was used in reactive powder concrete mix, which is made by AL-Nawafith Company in AL-Najaf. Light-weight aggregate (Leca) Structural lightweight aggregate has been used in lightweight concrete mix having a max size (8 mm), it has been provided from Mujemma AL-Bahrain contracting company in Al-Najaf. Silica Fume, mega Add MS(D) is a fine pozzolanic to use high performance mineral additive for use in reactive powder concrete mix, the properties of silica fume are provided from the manufacturer, which were in conforming with the specifications of ASTM C1240-03 [23].

Super plasticizer Mater Glenium 54, PH (5-8) has been used in concrete mixtures to make the mixture self-compacting and reduce the percentage of water, the production of very high early and high ultimate strength concrete with minimal voids, high workability without segregation or bleeding. It is used in all concrete mixes, correspond with the requirements of the super plasticizer determined by ASTM C- 494 Type F & G [24], which are equipped from the manufacturer. Lime stone is a white fine crushed powder known locally as (Al- Gubra) that has been used as filler material in self – compacting concrete. Straight micro steel fibers with diam. of 0.22 mm and length 13.1 mm have been used for the purpose of enhancing the shear resistance and improving the durability of the reactive powder concrete mix. Its tests complied with the requirements of ASTM A 820-06 [25], data are provided from the manufacturer.

Three different sizes of steel reinforcement have been used. Samples of reinforcing steel were tested in the Construction Laboratory of the University of Kufa, and the results were in line with the specifications ASTM A615 [26] as shown in Table 4.

**Table 2** Physical and chemical properties of the sand

No	Sieve size (mm)	Percentage of Passing	%Passing limits Zone (3) [22]
1	10	100	100
2	4.75	95.4	90-100
3	2.36	92.1	85-100
4	1.18	87.8	75-100
5	0.6	64.8	75-79
6	0.3	38.9	12-40
7	0.15	3	0-10
Materials Passing through a sieve 75 micron %		3.61	≤5
Chemical properties		Limits [22]	
Sulfate Content %		0.3	≤ 0.5

**Table 3** Physical and chemical properties of the gravel

Sieve Size (mm)	Percentage of Passing	%Passing limits [22]
37.5	100	100
20	95.53	95-100
10	32.67	30-60
5	1.37	0-10
Materials Passing through a sieve 75 micron %		≤ 3%
Chemical properties		Limits [22]
Sulfate Content (SO <sub>3</sub> )		≤ 0.1% 0.26%

**Table 4** Properties of steel reinforcement bars

diameter (mm)	Yield stress (MPa)	Tensile strength (MPa)
8	445	630
10	480	695
16	600	697

## 2.3 Tests of the Fresh Self –Compacting Concrete

Slump Flow and T500 Tests to estimate the flow ability of self-compacting concrete according to the ACI 237R-07 [27]. J-ring test is used to test the passing ability of self-compacting concrete (SCC). The slump flow and j-ring tests are shown in Figure 2 ASTM (C1621/C1621M) [28]. The results of the Test SCC listed in the Table 5.



a) J-ring test                      b) slump flow test

**Figure 2** SCC mix tests

**Table 5** The results of the Test SCC

Test	Results		Specification Limits
	NC	LWC	
Slump Flow (mm)	630	720	(450-760) [27]
T500 (sec)	3	3	(3-5) [27]
J-ring (mm)	35	37	(25-50) [28]

**2.4 Mechanical Properties of the Hardened Concrete**

The tests of hardened concrete were used in this study were carried out in the structural Laboratory of the Faculty of Engineering at the University of Kufa. The test has been done for cylinders with dimensions (150 mm diameter, 300 mm length) to evaluate the cylinder compressive strength ( $f_c$ ) according to ASTM C39/ C39-15a [29]. as well, cubes with dimensions (100X100X100) mm to evaluate the cube compressive strength ( $f_{cu}$ ) according to BS 1881-116 1983 [30]. Splitting tensile strength has been determined by testing three standard cylinders of (100 mm diameter, 200 mm length) ASTM C496 -11 [31]. Modulus of elasticity has been determined by testing three standard cylinders of (150 mm diameter, 300 mm length) ASTM C496-14[32]. Table 6 shows the results of tests for the various concrete mixes.

**Table 6** test results of hardened concrete

mix	Cube compressive strength ( $f_{cu}$ ) MPa	Cylinder compressive strength ( $f_c$ ) MPa	Splitting tensile strength ( $f_t$ ) MPa	Modulus of elasticity (E)GPa
RPC	93	76	9.1	39.3
NC	46	37	2.41	27.4
LWC	37	31	2.28	24.31

**2.5 Instrumentation for Testing and Testing Machine**

The crack width was measured with a crack meter with an accuracy of 0.5 mm. When the crack width

exceeded 0.5 mm, the crack was measured with a digital Vernia. Every 40 kN, the crack width was measured. Figure 3(a) shows the crack meter and Vernia. The deflection of the deep beam was measured at two points, mid face of the beam, is measured using (LVDT) as shown in Figure 3(b). Furthermore, the data logger device was used to record the load deflection data as shown in Figure 3 (c).



(a)                      (b)                      (c)

**Figure 3** Testing devices a) crack meters, b) LVDT, c) data logger

The universal test machine consists of two major components for testing reinforced concrete deep beams. The control panel and the loading unit. Each deep beam being tested receives the weight in small increments. Each load increment was 5 kN. More than 80 kN in 10 kN increments till failure. With each increment, the data logger's readings. A monotonic overload test was performed on all specimens until they failed. The evolution of the fracture is monitored at each step. From one step to the next, the crack width is measured. The loading mechanism and testing are shown in Figure 4.



**Figure 4** testing machine

### 3.0 RESULTS AND DISCUSSION

#### 3.1 Crack Patterns at Failure

Figure 5(a) shows the full map of cracking propagation for the control deep beam, CTRL-1P, close to the final stage of loading. It can be seen that the first crack initiated as flexural at load 70 kN within the mid span following vertical direction towards the point loads. This may be attributed to the distribution of the shear force (S.F.) and bending moment (B.M.) along the beam, and putting in mind that the beam is designed based on the strut and tie model STM adopted by ACI318M-19 [1] code. It can be observed that due to the reduction of B.M towards the supports, shear force effect increases gradually away from mid-span. More cracks develops on both sides of the center line with angle degreased gradually, up to reaching the smallest angle for the farthest crack (diagonal crack) at load 160 kN with angle of about 37°. Such crack represented the path of the compression forces which is termed as the compression strut that connected the point load with the supports reaction. Some crushing occurred at top fibers under the point load referring to high value of curvature before failure.

For G1-RN-1P specimen, Figure 5(b), it is expected that the failure of the control specimen was due to exhausting the compression force induced by the compression block due to the development flexural crack up, with progress a loading. Thus, the equilibrium between the tension and compression forces violated. Consequently, this model of hybrid beams is based on increasing the compressive resistance of the section by using reactive powder concrete at the top half of the beam. Then, more energy is needed such that the crack grows up and cause failure. It can be seen that the first crack initiated at the mid- span within a load stage of 90 kN. The rate of development of this crack is combated when reaching the RPC layer of concrete. Thus, more cracks developed on both sides within the bottom layer. However, the rate of growth of all cracks is slowed down when reaching the RPC layer. The curvature is restricted and rate of the lateral propagation of cracks is lower than the control specimen. This explain why the diagonal crack in specimen G1-RN-1P developed at load 180 kN. Failure occurred within load of 523 kN following mode of the flexural-shear type, recording an enhancement in capacity by 27.6% compared with control specimen, the failure of beam is accompanied by some crushing at supports. This local failure is expected to result in increasing rate of failure.

In the presently proposed model, Figure 5(c), it is aimed to control this problem by using the curved distribution of the high strength concrete RPC , and also reduce the weight by using lightweight concrete within the bottom layer (sector). It can be seen that

cracking initiated at load 80 kN as flexural type for specimen G2-RL-1P. However, the arching action and the high strength concrete RPC used restricted the excessive curvature and propagation and crack laterally. All of the inclined crack developed within the lightweight concrete, very small cracks developed within the area around it. The improved rigidity resulted in accommodation of higher loads. No crushing occurred under the applied load. The significance of the proposal model may be observed clearly with specimens of larger scales at which the ratio of the lightweight area will be increased gradually up to reached 60%. At load 570 kN, specimen G2-RL-1P failed by flexural failure. The use of the curved distribution of concrete led to an increase in the capacity of the deep beam to 39% and 9% compared to the control model and the horizontal hybrid model respectively, despite the use of lightweight concrete in the tension area.

When loading with two point loads, the moment at the middle part of the beam is constant and the shear force is zero. Therefore, the capacity of the deep beam increases compared to the specimens tested under one-point loading. For the control specimen CTRL-2P, the cracks appeared at the flexural area with a loading of 80 kN and propagated on the two sides as shown in the Figure 5(d). When the load reaches 140 kN, the first diagonal shear crack appeared within the shear span area. Some crushing occurs at the support area the final stages, followed by failure at load 542 kN. The beam capacity increases by 32.2%. When the load is distributed over two point loads instead of the application as one point load.

The hybrid specimen, beam G1-RN-2P, is similar to specimen G1-RN-1P with the exception that the two-point load system is used. Due to the distribution of shear force and bending moments along the beam, the first crack appeared as a flexural one when the loading reached 80 kN. With loading progress, more flexural cracks developed vertically at the region of zero shear within the bottom half of the beam because that the rate of development slowed down at the RPC area as it is observed in Figure 5(e). The shear cracks spread and the main diagonal crack by angle 50° is more inclined than the CTRL-2P pattern which its angle is 42°, meaning it is closer to the moment region due to the increased strength of struts region. Beyond the load of 300 kN, diagonal cracking developed close to the supports towards the compression face. At final stages of loading some crushing occurs at supports due to the severe intensity of stress. The failure occurs at 727 kN by a flexural-shear mode. It can be seen that improvement the performance of the strut areas, the capacity of the deep beam is increased by 34.1% compared to the control model.

For specimen G2-RL-2P, the hybrid distribution of this model is similar to that of G2-RL-1P. Figure 5(f) shows the crack propagation of the specimen at failure instant. When loading reached 60 kN, similar

behavior as in the specimen G2-RL-1P can be observed with the acceptance the region of the flexural vertical cracking is extended to include area between the two concentrated loads and that diagonal shear region is shifted towards the supports, then the diagonal cracking occurs with higher level of loading. Larger angles of inclination for the plane of diagonal mode was observed. The specimen fails at loading 742 kN with flexural failure. It is possible to increase the capacity of the beam and prevent failure by increasing the tensile reinforcement. The capacity of beam increased by 36.9% compared normal deep beam. Table 7 shows tests result of specimens. It can be concluded that the minimum limit for the steel area crossing the compression strut may result in flexural mode and the beam may fail following a ductile mode of failure.

**Table 7** Experimental test results of specimens

Specimen	Cracking load Pcr (kN)	Ultimate Load Pu (kN)	Max. Deflection (mm)	Mode of failure
CTRL-1P	70	410	13.8	Flexural-shear failure
G1-RN-1P	90	523	16.07	Semi-flexural failure
G2-RL-1P	80	570	21.01	Flexural failure
CTRL-2P	80	542	12.23	Flexural-shear failure
G1-RN-2P	80	727	24.49	Flexural-shear failure
G2-RL-2P	60	742	33.62	Flexural failure

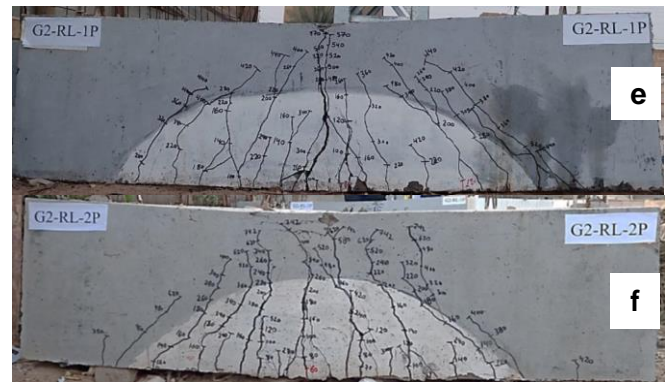
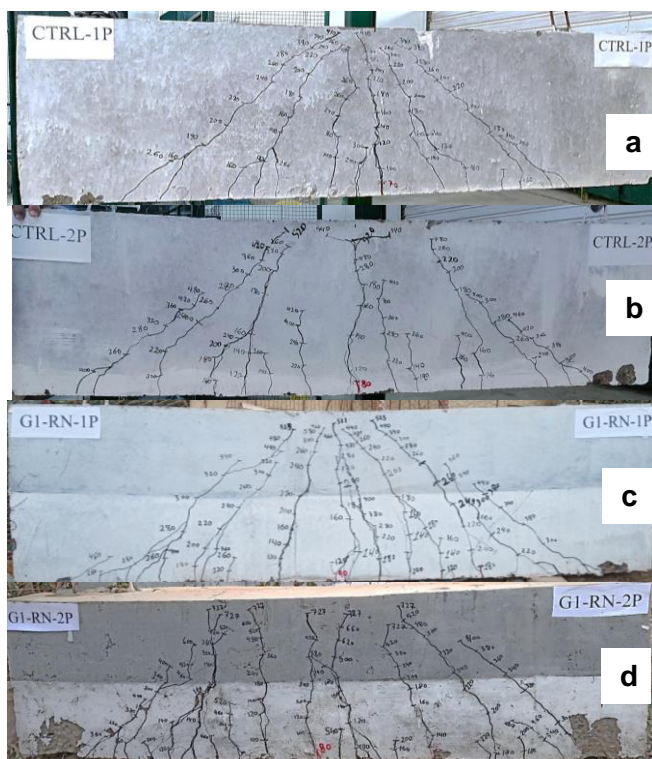


**Figure 5** Crack Patterns for the: a) CTRL-1P, b) CTRL-2P, c) G1-RN-1P, d) G1-RN-2P, e) G2-RL-1P, f) G2-RL-2P

### 3.2 Crack Width

Figure 6(a) shows the rate of crack widening with loading progress for the specimens tested under one point load. It is clear that rate of widening of the flexural cracks is more than that for the diagonal one. This may be attributed to the STM design method, which recommend using a minimum value for steel crossing the compression strut. Such steel represent the shear reinforcement i.e. using steel amount more than the minimum limit may transfer the deep beam to be controlled by flexural failure. Results also, show that the rate of widening for the control specimen is higher than the other two specimens for the two types of cracks, thus may be attributed to the effect of the RPC used. Moreover, it can be observed that the proposed model yielded lower rate of widening for the diagonal crack and better restriction for widening for the flexural crack. Moreover, it can be seen that the two models of hybridization yielded same rate of crack widening up to a load of 450 kN, beyond which the proposed model yielded better responses.

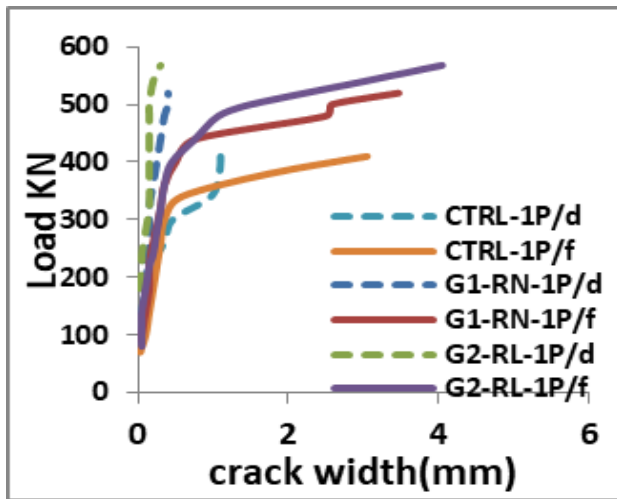
For the specimens tested under two point loading, the rate of crack widening are depicted in Figure 6(b). Results prosed that the three specimens tend to failing diagonal cracking mode more than the corresponding specimens testing under one point loading. Moreover, it can be observed that the control specimens yielded the highest rate of crack widening. For the specimen with the conventional model of hybridization, the lowest rate of widening of cracks can be seen this may be attributed to that the diagonal crack in addition to the flexural cracks occurred at the lightweight concrete. However, the arching action provided by the arched of the RPC reduce the difference between the two hybrid models. This is very clear in the diagonal crack rather than the flexural crack.

### 3.3 Load-deflection Curves

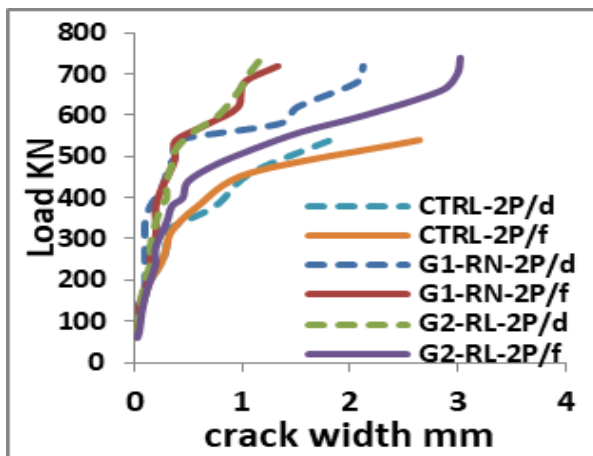
Figure 7(a) shows the loading histories for the deep beams tested under one point load. Results revealed

that the conventional hybrid beam yielded improvement in capacity by (27.6%) while that the proposed model resulted in enhancement of (39%). It is also obvious that the control and conventional hybrid beam yielded the same initial stiffness while the proposed model showed higher stiffness and rigidity. The relation between load and deflection refers to the safety indications i.e. toughness and ductility which may be improved accordingly.

For two point loads Figure 7(b) shows the load deflection curve for the beam tested under two point loads results proved that the enhancement in capacities of (34%) and (36.9%) for the two hybrid beams respectively. Moreover, it can be seen that the three specimens had the same initial and final stiffness. Thus, it can be calculated that the application of load on several points reduced the intensity of stress and controlled the severity of disturbance.

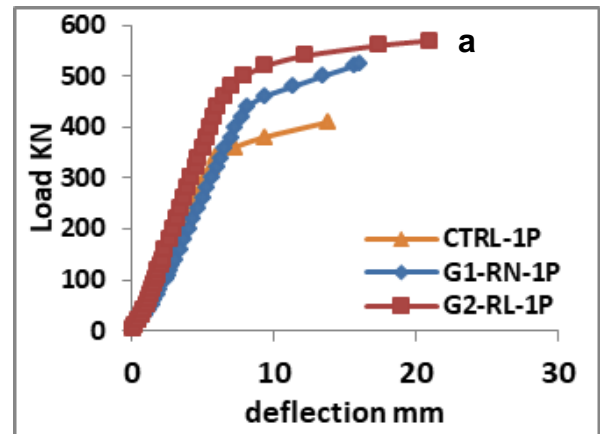


(a)

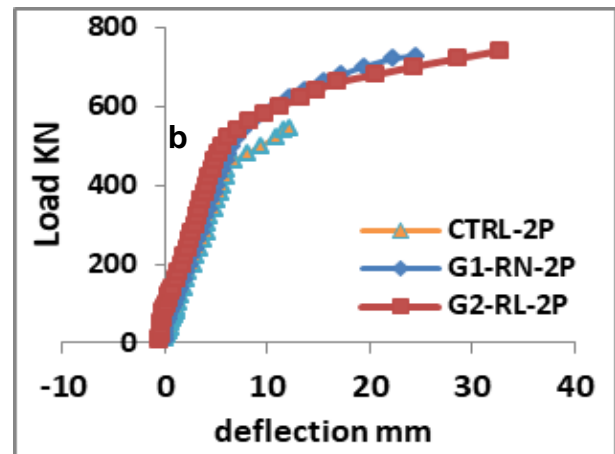


(b)

Figure 6 Crack width a) one point load, b) two point loads



(a)



(b)

Figure 7 Load-deflection curve a) one point load, b) two point loads

### 3.4 Toughness, Stiffness and Ductility

Toughness is a measure of a member's resistance to distortions prior to failure, which is represented by the area under the curve [33]. The control specimens CTRL-1P, CTRL-2P have the lowest toughness, which is 3908 kN\*mm and 4413 kN\*mm respectively. When using the RPC layer for the conventional hybrid G1-RN-1P and G1-RN-2P, the toughness improved by 44% and 188.5% respectively compared with control specimens, because that the RPC covers most of the struts area. For specimens G2-RL-1P, G2-RL-2P, the increase was even more because the high strength concrete included all D-region of the deep beam, where it increased by 131% and 301% respectively, compared to the reference models.

Stiffness (K) is a measure of the resistance offered by an elastic body to deformation. The "effective secant stiffness" is used corresponding to load stage (0.75\*Pu) [34]. The value of stiffness for the control specimen was lower from all specimens. Additionally, it can be noted that the conventional hybrid deep beam G1-RN-1P, G1-RN-2P have a stiffness that is approximately 6.5% and 7.5% respectively, greater than the control specimens. It can also be noted that

the arched hybrid model G2-RL-1P and G2-RL-2P showed an increase in the stiffness of about 34.2% and 29.4%, respectively compared to the reference beams, due to the effectiveness of using high strength concrete at the strut area in the improvement of the stiffness.

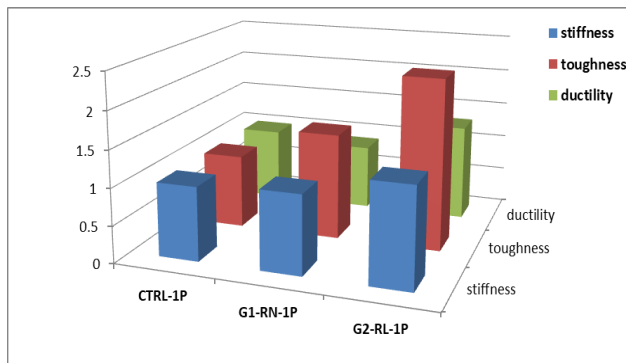
Ductility the ability to resist inelastic deformation without diminishing ultimate load till failure and it can be expressed as in Eq. (1) [35]. Table 3 shows results of toughness, stiffness and ductility.

$$\mu = 0.5 * (E_{tot}/E_{el} + 1) \quad \text{Equation (1)}$$

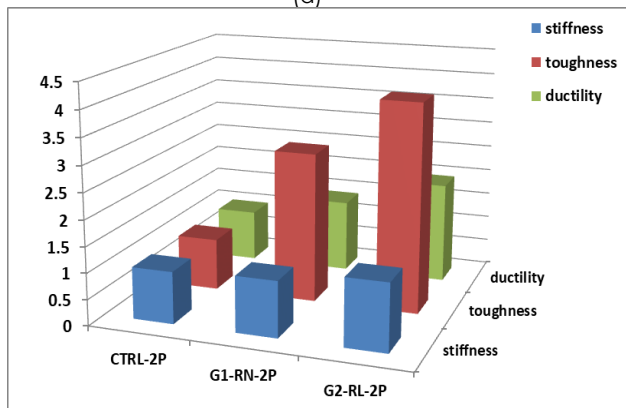
$E_{tot}$ : area under the full load-deflection curve and  $E_{el}$  is the area under the elastic part on layer elastic part only. It was noted that using RPC in the upper half of the deep beam G1-RN-2P specimens, increased the ductility by 40.37% compared control specimen. Whereas, the ductility for the specimens by curved distribution of steel fiber concrete, G2-RL-1P, G2-RL-2P was 31.18 %, and 95.1% respectively, compared the control specimens. The results shown in Table 8 and Figure 8.

**Table 8** Results of toughness, stiffness and ductility

specimen	toughness	Stiffness	ductility
CTRL-1P	3908	55	1.83
G1-RN-1P	5627	58.6	1.66
G2-RL-1P	9030	73.8	2.41
CTRL-2P	4413	69	1.63
G1-RN-2P	12731	74.2	2.29
G2-RL-2P	17713	89.3	3.18



(a)



(b)

**Figure 8** results of toughness, stiffness and ductility a) one point load, b) two point loads

## 4.0 CONCLUSION

The capacity of the deep beam increased in the horizontal and the arched hybrid model by 27.6% and 39%, respectively, compared to the reference model when loading with one- point, and by 34% and 36.9%, respectively, when loading under two - points.

When changing the loading type from one point to two point, the beam capacity increased for the control, horizontal hybrid and arched hybrid by 32.2%, 39% and 30.2% respectively.

When the loading systems of one point load, for horizontal hybrid and arched hybrid deep beam, toughness increased by 44% and 131% respectively. Whereas enhancements in stiffness by 6.5% and 34.2% respectively are observed. Regarding ductility, an improvement of 31.2% was seen for the arched hybrid model and some reduction for the horizontal hybrid model. When the loading systems of two point loads, for horizontal hybrid and arched hybrid deep beam Toughness increased by 188% and 301% respectively. Regarding stiffness, enhancements by 7.5% and 29.4% respectively whereas for ductility, the improvements were 40.3% and 95.1% respectively.

Using of lightweight concrete in the tie region of the deep beam did not affect the capacity and the overall behavior of the deep beams.

Test results also revealed, that the design of steel reinforcement crossing the compression strut for the deep beams as recommended by the STM models may result in some ductile behavior and beams may fail by flexural cracking.

## Acknowledgment

The authors are grateful to the Construction and Structures Laboratories of the University of Kufa for their valuable support for this research program.

## References

- [1] A. Committee. 2019. 318M-19: Building Code Requirements for Concrete and Commentary. 628.
- [2] Shakir, Q. M. and Abdlsaheb, S. D. 2022. Rehabilitation of Partially Damaged High Strength RC Corbels by EB FRP Composites and NSM Steel Bars. *Structures*. 38: 652-671.
- [3] Shakir, Q. M. 2020. Response of Innovative High Strength Reinforced Concrete Encased-composite Corbels. *Structures*. 25: 798-809.
- [4] Mata-Falcón J., Pallarés L. and Miguel P. F. 2019. Proposal and Experimental Validation of Simplified Strut-and-tie Models on Dapped-end Beams. *Engineering Structures*. 183: 594-609.
- [5] Shakir, Q. M., Alliwe, R. 2021. Strengthening the Self Compacting Reinforced Concrete Dapped Ends with Near Surface Mounted (NSM) Steel Bar Technique. *IJASEIT Journal*. 11(2): 663-673.
- [6] Desnerck, P., Lees, J. M. and Morley, C. T. 2018. Strut-and-tie Models for Deteriorated Reinforced Concrete Half-joints. *Engineering Structures*. 161: 41-54.

- [7] Katalin, H., Eva, L. 2013. Investigation of Steel Fibers Bond Strength in Mortar Matrix. *Pollack Periodica Journal*. 8(3): 101-110.
- [8] Naser, K., Cene, K., Enes, K. and Vlorian, K. 2018. Comparison of the Behavior of GFRP Reinforced Concrete Beam with Conventional Steel Bars. *Pollack Periodica Journal*. 13(3): 141-150.
- [9] Gouveia, N. Dm, Lapi, M. O., Faeia, D. M. and Ramos, A. M. 2018. Exeperimental and Theoritical Evaleuation of Punching Strength of Steel Fiber Reinforced Concrete Slabs. *Structural Concrete Journal*. 19(1): 217-229.
- [10] Campione, G., Mendola, L. La, Mangiavillano, M. L. 2007. Steel Fiber-reinforced Concrete Corbels: Experimental Behavior and Shear Strength Prediction. *Structural Journal*. 104(5): 570-579.
- [11] Shakir, Q. M., Hamad, S. A. 2021. Behavior of Pocket-Type High-Strength RC Beams without or with Dapped Ends. *Pract. Period. Struct. Des. Constr.* 26(4): 1-12.
- [12] Hamad, S. A, and Shakir Q. M. 2021. Behaviour of RC Beams with Strengthened Web Openings under Vertical Loads. *IOP Conf. Series: Materials Science and Engineering*. 1094: 012062.
- [13] Isojeh B., El-Zeghayar, M., and Vecchio, B. J. 2017. Fatigue Resistance of Steel Fiber-reinforced Concrete Deep Beams. *ACI Struct. J.* 114(5): 1215-1226.
- [14] Birincioglu, M. I. and Arslan, G. 2019. Evaluation of Shear Strength Approaches of SFRC Deep Beams without Stirrups. *Technol. Eng. Math.* 7(1987): 131-135.
- [15] Hassan, F. H. 2015. Behavior of Hybrid Deep Beams Containing Ultra High Performance and Conventional Concretes. *Eng. Tech. J.* 33(1): 30-50.
- [16] Sada, M. J. and Resan, S. F. 2021. Shear Performance of Hybrid Concrete Deep Beams of Trapezoidal Section. *IOP Conf. Ser. Mater. Sci. Eng.* 1067(1): 1-19.
- [17] Al-Attar, A. A., Abdulrahman, M. B., Hamada, H. M. Tayehd, B. A. 2020. Investigating the Behaviour of Hybrid Fibre-reinforced Reactive Powder Concrete Beams after Exposure to Elevated Temperatures. *Journal of Matirials Research and Technology*. 9(2): 1966-1977.
- [18] Hadi, M. N. S., GOALZ, H., and Yu, T. 2018. Experimental Investigation of CFRP Confined Hollow Core Reactive Powder Concrete Columns. *Construction and Building Materials*. 174: 343-355.
- [19] Muhaison, S. K., Abd. W. K., Alwan M. K. 2018. Behaviour of Reactive Powder Rectaingular Deep Beams with Shear Zone Opening Subjected to Repeated Load. *Journal of Engineering and Sustainable Development*. 22(1): 77-94.
- [20] Shakir, Q. M. and Hannon, H. K. 2023. Behavior of High Performance Reinforced Concrete Hybrid Deep Beams. *Jestec Journal*. 18(1).
- [21] Iraqi Specification No. 5. 1984. Portland Cement. Baghdad.
- [22] Iraqi Specification No.45. 1984. Natural Sources for Gravel that is Used in Concrete and Construction, Baghdad.
- [23] ASTM C1240-03. 2003. Standard Specification for the Use of Silica Fume as a Mineral Admixture in Hydraulic Cement Concrete. *Mortar and Grout*. 4(2): 6.
- [24] ASTM C494/C494M-13. 2013. Standard Specification for Chemical Admixtures for Concrete. Annual Book of ASTM Standard.
- [25] ASTM A 820-06. 2006. Standard Specification for Steel Fibers for Fiber Reinforced Concrete 1. 1-4.
- [26] ASTM A615/A615M-04. 2004. Standard Specifications for Deformed and Plane Carbon-Steel Bars for Concrete Reinforcement. Annual Book of ASTM Standard.
- [27] ACI Committee 237R-07. 2007. ACI 237R-07 Self-Consolidating Concrete. Farmington Hills, Michigan; American Concrete Institute.
- [28] ASTM C1621/C1621M-14. 2014. Standard Test Method for Passing Ability of Self-Consolidating Concrete by J- Ring. Annual Book of ASTM Standard.
- [29] ASTM C39/C39M-15a. 2015. Standard Test Method for Compressive Strength of Cylindrical Test Specimens. Annual Book of ASTM Standard.
- [30] BS 1881-116. 1983. Method for Determination of Compressive Strength of Concrete Cubes. British Standards Institute, London.
- [31] ASTM C496/C496M-11. 2011. Standard Test Method for Splitting Tensile Strength of Cylindrical Concrete Specimens. Annual Book of ASTM Standard.
- [32] ASTM C469/C469M-14. 2014. Standard Test Method for Static Modulus of Elasticity and Poisson's Ratio of Concrete in Compression. Annual Book of ASTM Standard.
- [33] Shakir, Q. M., and Abd, B. B. 2020. Retrofitting of Self Compacting RC Half Joints with Internal Deficiencies by CFRP Fabrics. *Jurnal Teknologi*. 82(6): 49-62.
- [34] Park, R. 1988. Ductility Evaluation from Laboratory and Analytical Testing. *Proceedings of the 9th World Conference on Earthquake Engineering*. 605-616.
- [35] Naaman A. and Jeong S. 1995. Structural Ductility of Concrete Beams Prestressed with FRP Tendons. *Proc. Second Int. RILEM Symp. (FRPRCS- 2) Non-Metallic Concr. Struct. Ghent, Belgium*. 379- 86.